High-Energy Astrophysics

Andrii Neronov

October 2, 2017

Contents

Chapter 1

Introduction

The term *"High-Energy Astrophysics"* combines two keywords which determine the scope of the subject.

The "High-Energy" physics conventionally deals with the world of high-energy particles, i.e. particles with energies much higher than the rest energy. For electrons the rest energy is

$$E = m_e c^2 \simeq 5 \times 10^5 \text{ eV} \tag{1.1}$$

(here $m_e = 0.9 \times 10^{-27}$ g is the mass of electron and $c = 3 \times 10^{10}$ cm/s is the speed of light), while for proton it is

$$E = m_p c^2 \simeq 10^9 \text{ eV} \tag{1.2}$$

with the proton mass $m_p = 1.6 \times 10^{-24}$ g. In laboratory conditions here on Earth, the high-energy particles are produced by accelerator machines, like the Large Hadron Collider (LHC) at CERN, in which protons reach energies in the range of 10 TeV. The main goal of the High-Energy Physics research is to understand the fundamental constituents of matter (elementary particles) and interactions between them.

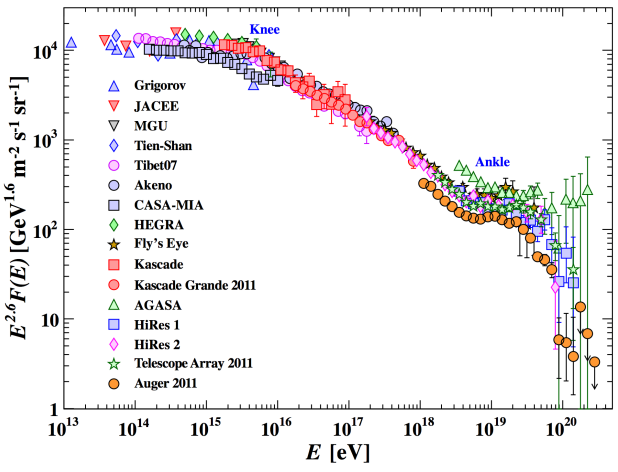

Figure 1.1: The spectrum of cosmic rays measured by different experiments. This log-log scale plot shows the differential flux of particles per unit energy interval, $F(E)$, multiplied by energy E to the power 2.6. From Ref. [4].

Second part of the name High-Energy Astrophysics contains the word *"Astrophysics"* which clearly refers to astronomical observations, typically done using various types of telescopes and aimed at understanding of the properties and mechanisms of activity of different types of astronomical sources, like stars and galaxies.

Combining the two parts into one subject defines the subject of High-Energy Astrophysics as research in the domain of Astronomy, specifically aimed at understanding of the role of high-energy particles and their interactions in the activity of different types of astronomical sources.

The fact that some astronomical objects work as particle accelerators is established based on two types of observational data.

First, we directly detect the high-energy charged particles coming from space in the form of *cosmic rays*. Measurements of the spectrum of cosmic rays (Fig. 1.1) show that the energies of the cosmic ray particles reach 10^{20} eV, which is some seven orders of magnitude higher than the maximal energies of protons attained at the LHC.

These particles are produced by some (still unknown) astronomical sources and it is one of the major challenges of modern physics and astronomy to identify these sources. The uncertainty of the sources of cosmic rays constitutes the long-standing *problem of the origin of cosmic rays*. The cosmic rays were first discovered in 1912, so the problem is now 100-year-old.

Next, the information on the presence of high-energy particles in astronomical sources is obtained indirectly, via observations of those sources with telescopes operating at different wavelengths, i.e. with the tools of the *"multi-wavelength astronomy"*. From the early days of the mankind, people have started to do astronomical observations, by looking at the stars on the sky first with the naked eye, and then, starting from Copernicus, with telescopes. Up to the middle of 20th century, the word "astronomical observations" was synonymous to the "astronomical observations in the visible band", because the only type of light sensors used was the human eye, sensitive in the visible range. The visible energy band contains photons in the wavelength range

$$400\text{nm} \leq \lambda \leq 700 \text{ nm} \tag{1.3}$$

This corresponds to a rather narrow range of photon energies $\epsilon = 2\pi\hbar c/\lambda$

$$1.8 \text{ eV} < \epsilon < 3.2 \text{ eV} \tag{1.4}$$

Only astronomical sources emitting photons in this specific energy range were known all this time.

Starting from the end of 1960's, the tools of radio, infrared, ultraviolet, X-ray and gamma-ray astronomy started to develop, so that today, just 50 years after, the energy range available for the astronomical observations comprises some 12 decades in energy:

$$10^{-6} \text{ eV} < \epsilon < 10^{13} \text{ eV} \tag{1.5}$$

Fig. 1.2 shows the definition of different "energy windows" of the multi-wavelength astronomy.

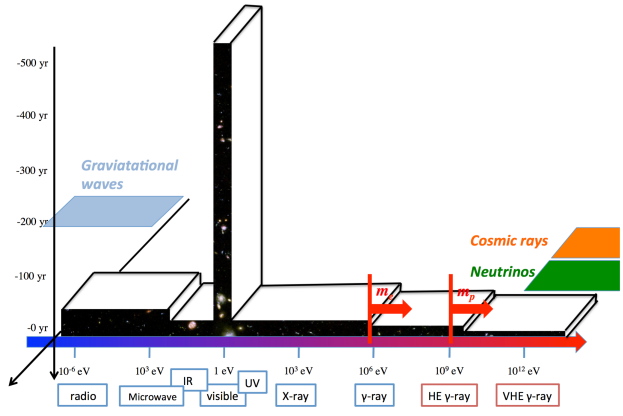

Figure 1.2: Timeline of the history of astronomy and definition of different energy / wavelength bands. and different astronomical "messenger" particles.

The tools of the multi-wavelength astronomy have opened a possibility of observing the effects of interactions of high-energy particles in astronomical sources. Photons with energies up to 10^{13} eV are produced by particles with energies at least $E > 10^{13}$ eV, i.e. much higher than the rest energies of proton and electron. These particles emit photons of different energies, from radio to γ-rays via a variety of emission mechanisms: synchrotorn, Compton scattering, Bremsstrahlung, pion production and decay. Combinaiton of multi-wavelength data is important for getting a complete picture of physical mechanisms of activity of the sources.

In a similar way, the high-energy sources also emit different types of particles, "astronomical messengers". Apart from photons, the most common "astronomical messenger" particles, information on mechanisms of operation of high-energy sources is also carried by neutrinos, cosmic rays and gravitational waves. Combinaiton of the "multi-messenger" data (Fig. 1.2) is equally important for understanding of the mechanisms of operation of sources.

In the context of the multi-wavelength astronomy, the term "High-Energy Astrophysics" is sometimes understood in a slightly different sense, than explained above. the term "High-Energy" might also refer to "photons energies higher than those of the visible / UV light". In this case the "High-Energy Astrophysics" research field comprises all possible sources and physical processes which manifest themselves through the X-ray and gamma-ray emission. This includes then not only processes

related to the presence of relativistic particles in the sources, but also thermal processes in astronomical objects with temperatures in the range above 100 eV (the low-energy boundary of the X-ray band).

1.1 Types of astronomical HE sources

Large part of astronomical sources emit radiation with thermal spectrum characterised by temperature T. The energies of particles generating this radiation could be estimated from the well-known relation

$$\langle E \rangle \sim \frac{3}{2} k_B T \tag{1.6}$$

where $k_B = 8.6 \times 10^{-5}$ eV K^{-1} is the Boltzmann constant serving as a conversion coefficient between the units of temperature and energy units. Presence of relativistic particles in the thermal astronomical objects implies the temperature range

$$T \sim \frac{m_e c^2}{k_B} \simeq 0.6 \times 10^{10} \text{ K} \tag{1.7}$$

for the objects containing relativistic electrons or

$$T \sim \frac{m_p c^2}{k_B} \simeq 10^{13} \text{ K} \tag{1.8}$$

for the objects with high-energy protons.

The temperature range $T \sim 10^{10}$ K might be reached in the interiors of stars or at the final stage of life of massive stars when they explode as supernovae. The surface temperatures of the stars are typically much lower, not exceeding 10^5 K, so that solar-like and massive stars powered by the nucleosynthesis reactions are not the sources of interest in the High-Energy Astrophysics domain.

Much higher temperatures are sometimes reached in the objects powered by the release of gravitational (rather than nuclear) energy. A typical first estimate of the temperature of a gravitationally collapsing matter is given by the virial theorem

$$T \sim \frac{2}{3} \frac{\langle E \rangle}{k_B} \sim \frac{1}{3} \frac{U}{k_B} \sim \frac{G_N M m_p}{3 k_B R} \tag{1.9}$$

where $G_N = 6.7 \times 10^{-8}$ cm^3/(g s^2) is the gravitational constant, M, R are the mass and size of the collapsing matter configuration and U is the gravitational potential energy. Typical particle energies become relativistic, $\langle E \rangle \sim m_p c^2$, if the body is compact enough, with the size

$$R \sim \frac{G_N M}{c^2}. \tag{1.10}$$

This size estimate is about the gravitational radius of a body with the mass M

$$R_{grav} = \frac{G_N M}{c^2} \simeq 1.5 \times 10^5 \left[\frac{M}{M_\odot} \right] \text{ cm}. \tag{1.11}$$

Objects of the size comparable to the gravitational radius are called "compact objects". The known astronomical compact object classes are *neutron stars* and *black holes*, including the supermassive black holes in the centres of galaxies and stellar mass black holes.

These two classes of objects are powering most of the astronomical sources studied in High-Energy Astrophysics, including

- Active Galactic Nuclei (AGN):

  - Seyfert galaxies (Sy)
  - quasars / blazars (QSO)
  - radio galaxies
- X-ray binaries (XRB):
  - Low-mass X-ray binaries (LMXRB)
  - High-mass X-ray binaries (HMXRB)
  - Micorquasars
- end products of the life cycle of massive stars:
  - supernova remnants (SNR)
  - pulsars and pulsar wind nebulae (PWN)
  - gamma-ray bursts (GRB)

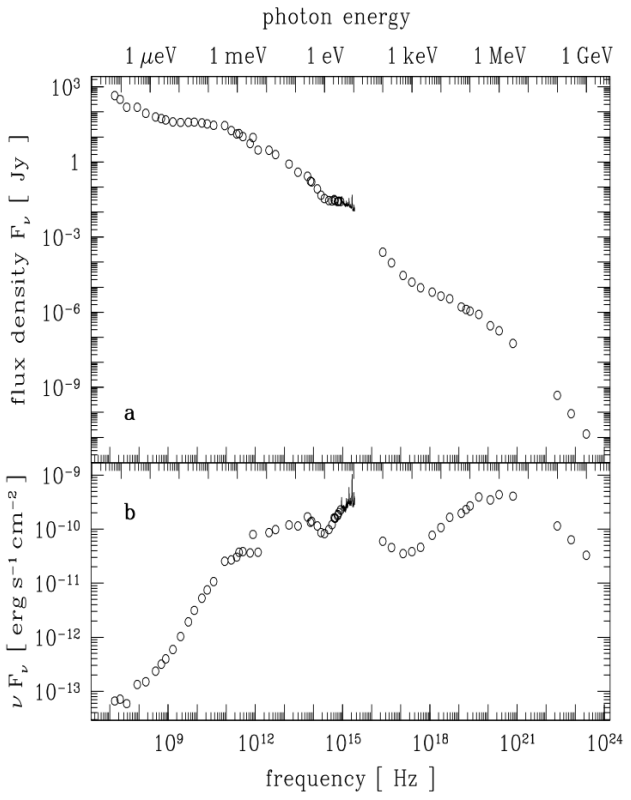

Figure 1.3: Spectral energy distribution of the quasar 3C 273, in two representations. The upper plot shore the differential flux, which is energy flux per unit energy or frequency. This flux is measured in the units of Jansky, 1 Jy= 10^{-23} erg/(cm^2 s Hz). The lower panel show the energy flux as a function of energy. From the Ref. [5].

Observations using the tools of multi-wavelength astronomy show that significant part of High-Energy Astrophysics sources does not emit radiation with thermal spectrum. Instead, they reveal signal which is spread over many decades of energy. Fig. 1.3 shows an example of such broad band spectrum in the quasar 3C 273. The broad range of photon energies is explained by the broad range of the energies of charged particles (electrons, protons) which have produced the photons. In the particular case of 3C 273, one could see that particle energies should be spread over several decades in energy.

1.2 Types of physical processes involved

High-energy particles with broad energy distribution usually loose their energy via various radiative energy loss channels, before being able to "thermalise" (i.e. to establish thermal distribution in momenta). The main radiative (ie. "accompanied by photon production") energy loss channels for electrons are

- synchrotron / curvature radiation,
- inverse Compton emission,
- Bremsstrahlung

A non-radiative energy loss especially important for mildly relativistic and non-relativistic electrons is

- Coulomb (ionisation) energy loss

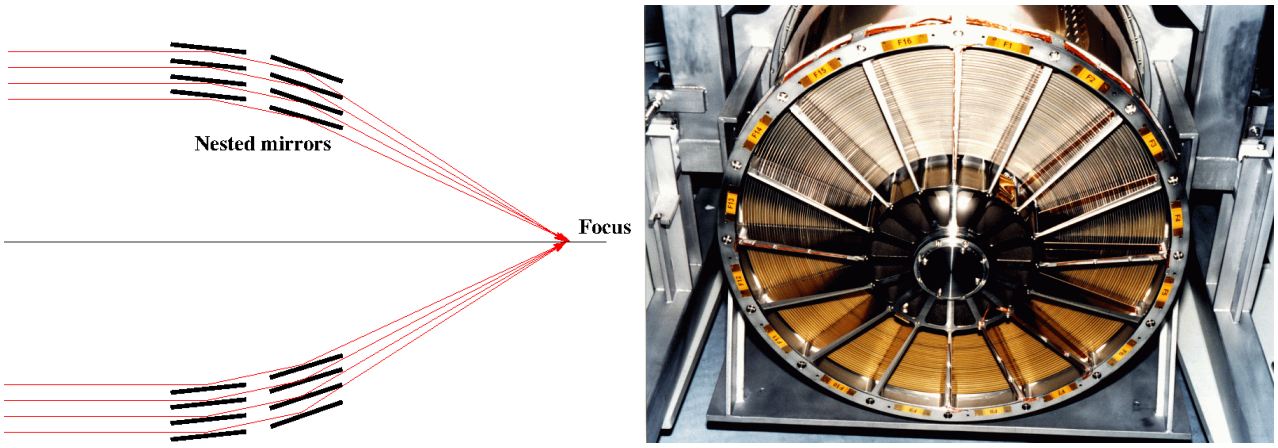

Figure 1.4: Left: the principle of grazing incidence optics used in X-ray telescopes. Right: the set of nested mirrors of the X-ray telescope *XMM-Newton*.

All these radiative and non-radiative channels contribute to larger or smaller extent to the formation of spectra of high-energy particles in the sources and to the formation of the broad-band emission spectra of the type shown in Fig. 1.3 for the quasar 3C 273.

In the case of high-energy protons the main radiative energy loss channel is

- production and decay of neutral and charged pions in interactions with matter and radiation fields.

The non-radiative Coulomb losses are also important for the lower energy mildly relativistic protons.

1.3 Observational tools

A complete understanding of the physics of sources with photon emission spectra extending from radio to gamma-rays (like 3C 273, shown in Fig. 1.3), is possible only with the detailed information on the imaging, spectral and timing information in all energy bands. This means that the observational tools of High-Energy Astrophysics include telescopes across all energy bands, including radio, infrared, visible, UV, X-ray and gamma-ray bands.

However, the term "experimental / observational High-Energy Astronomy" is usually reserved for telescopes and observational techniques in the X-ray and gamma-ray bands, with the visible / infrared astronomy and radio astronomies considered to be separate disciplines on their own.

X-rays and gamma-rays do not reach the ground. Observations in the X-ray and gamma-ray bands are, therefore, possible only with telescopes placed outside the Earth atmosphere in space. This explains why the age of High-Energy Astronomy has started only at the end of 1960th with the invent of the space flight.

Another peculiarity of the telescopes used in High-Energy Astronomy stems from the fact that, contrary to radio-infrared-visible radiation, X-ray and gamma-ray photons tend to interact with the telescope material in a destructive way, so that it is difficult to focus the signal with the conventional lenses / mirrors without destroying the photons. This is explained by the fact that the energy of each photon is comparable of higher than the ionisation energy of atoms composing the lens / mirror. As a result, the collisions of photons with atoms are inelastic and destructive.

This problem is partially overcome in the X-ray telescopes, where a special type of optical setup enables focusing of X-ray photons with energies up to 10 keV. The principle of the setup, known under the name of "grazing incidence optics", is shown in Fig. 1.4. To avoid the destructive interaction of X-rays with the lens / mirror material, the X-ray photons are falling on the mirror surfaces at large

incidence angles ("grazing" angles). A single grazing incidence focusing mirror (which could be e.g. segments of parabola) would have very small collection area, because it would intercept only a small faction of the X-ray photons. Stacks of nested mirror segments are used to achieve significant collection areas (in the range of $\sim 100 - 1000$ cm^2) with the grazing incidence technique. The right panel of Fig. 1.4 shows an example of the mirror of the X-ray telescope XMM-Newton, which is a European Space Agency (ESA) mission now in orbit.

Focusing photons of higher and higher energies would require the nested mirror systems with smaller and smaller grazing incidence angles. This, in turn, would imply larger and larger focal lengths. Thus, the grazing incidence technique stops to work at high energies (nowadays about 50 keV, achieved with the NASA X-ray telescope Nu-STAR). At higher energies astronomical observations are done without the use of focusing.

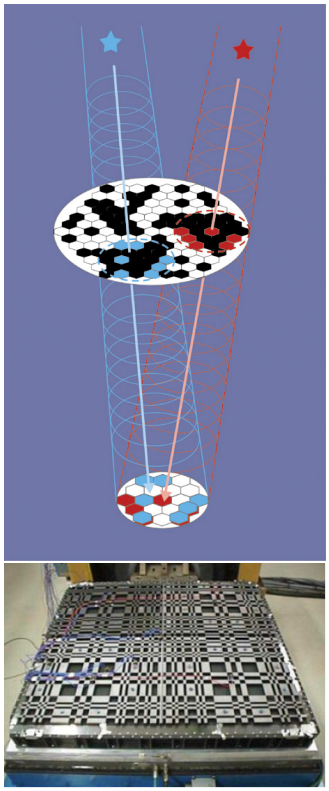

Figure 1.5: The principle of the coded mask optics and the coded mask of IBIS telescope on board of *INTEGRAL*.

One example of non-focusing optics is the "coded mask" technique, which is a direct development of the method of pinhole camera. This technique is illustrated in Fig. 1.5. Signal from an astronomical source passing through the mask (a plane with a set of holes) casts a particular shadow pattern on the detector plane. Registering this shadow pattern one could determine the source position on the sky via a straightforward ray tracing. Shadow patterns cast by different sources in the field of view overlap, but they are recognisable one-by-one, so that the ray tracing could be done for each source separately. This technique is used in a number of telescope currently operating in the hard X-ray / soft gamma-ray band, including the ESA INTergnational Gamma Ray Laboratory (INTEGRAL). The coded mask of the IBIS imager on board of INTEGRAL is shown in Fig. 1.5.

At the energies higher than ~ 1 MeV even the coded mask imaging would not work, because it would require a prohibitively heavy and thick mask which would be able to block gamma-rays. In this energy band telescopes do not use any imaging equipment at all. Instead, each gamma-ray is individually detected and it energy and arrival direction is determined. The observational data consist of the lists of gamma-rays detected from a given region of the sky in a given time span. Positions of sources of gamma-rays on the sky are identified by the clustering of large number of gamma-rays coming from particular directions. This principle of observations is used e.g. by the Fermi gamma-ray telescope operating in the 0.1-100 GeV energy band. Its setup is shown in Fig. 1.6. High-energy gamma-rays entering the telescope are converted into electron-positron pairs in one of the layers of the Tracker (the upper multi-layer part of the detector in Fig. 1.6). Trajectories of electron and positron are "tracked" by the Tracker and then energies of both particles are measured by the Calorimeter, which is the lower thicker layer of the detector shown in Fig. 1.6.

At the energies higher than ~ 100 GeV, the space-based detectors are unable to perform sensible astronomical observations, because of their limited collection area. In this energy band, each photon carries macroscopic energy (100 GeV=0.16 erg). The power of astronomical sources is carried by a small number of highly energetic photons and the overall number of photons rapidly decreases with the increase of the energy of each photon. Typical luminosities of astronomical sources are such that in the energy band above 100 GeV only about one or less photons per year could be detected by an instrument with collection area about 1 m^2.

Astronomical observations in the Very-High-Energy (VHE) band (photon energies above 100 GeV) are possible only with setups with extremely large collection areas (in the range of $10^4 - 10^6$ m^2). Such collection areas are provided by the ground-based Cherenkov telescope arrays, see Fig. 1.7.

The principle of detection of VHE gamma-rays is based on the fact that these gamma-rays produce electromagnetic cascades when they penetrate in the atmosphere. High-energy particles in the cascade move with the speed faster than the speed of light in the air and produce Cherenkov radiation in the UV wavelength range. Large optical reflectors are used to sample this Cherenkov light which appears for short periods of time (about ten nanoseconds) as bright "traces" of the gamma-ray induced cascade in the UV light. The information on the arrival direction and energy of the initial VHE gamma-ray is obtained via stereoscopic imaging of the cascade in the atmosphere (see Fig. 1.7, left panel). Right panel of Fig. 1.7 shows a 17 meter dish of the MAGIC telescope as an example of the large reflectors used by the Cherenkov telescopes.

1.4 Natural System of Units

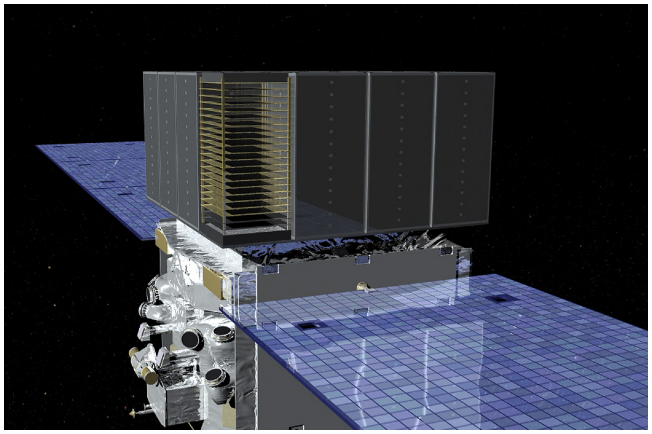

Figure 1.6: Fermi LAT telescope. The upper part of the telescope made of many layers is the Tracker. The lower thick layer part is Electromagnetic Calorimeter.

High-Energy Astrophysics subject relates particle physics and astronomy. These two branches of science use different unit conventions and it is sometimes challenging to convert the "language" of particle physicists into the "language" of astronomers and vice versa. A convenient approach is to reduce both astronomical and particle physics quantities and formulae to put them into a common unit system. Thoughout this course the common system of units will be the Natural System of Units, with the Gaussian version for electromagnetic quantities (as opposed to Heaviside-Lorentz, with quantities typically differing by 4π factors between Gaussian and Heaviside-Lorentz systems, see discussion in Ref. [6]).

The idea of the Natural system of units is to reduce the number of fundamental constants to the necessary minimum. This implies typically getting rid of the constants serving for unit conversions. For example, the Boltzman constant k_B serves for conversion between the units of temperature (which is, in essence a measure of energy) and energy:

$$k_B = 8.6 \times 10{-}5 \text{ eV K}^{-1} = 1 \tag{1.12}$$

This means that in the Natural system of units the temperature is always measured in electronvolts, instead of Kelvins. Whenever a measurement is provided in Kelvins, one immediately converts it into electronvolts using the relation

$$1 \text{ K} = 8.6 \times 10^{-5} \text{ eV} \tag{1.13}$$

The same is done with the electric and magnetic permeabilities of vacuum, encountered in the International System of Units:

$$4\pi\epsilon_0 = 4\pi\mu_0 = 1 \tag{1.14}$$

which serve for the introduction of the charge units (Coulomb) in this system.

In a similar way, one could see that the speed of light is, in a sense, a constant for conversion of the units of time and distance: one could measure distance in time units, with the unity the distance travelled by photons in one second, or, vice versa, once could measure time in the distance units, with the unity being time in which photon crosses the distance of 1 cm. Thus, imposing

$$c = 3 \times 10^{10} \text{ cm/s} = 1 \tag{1.15}$$

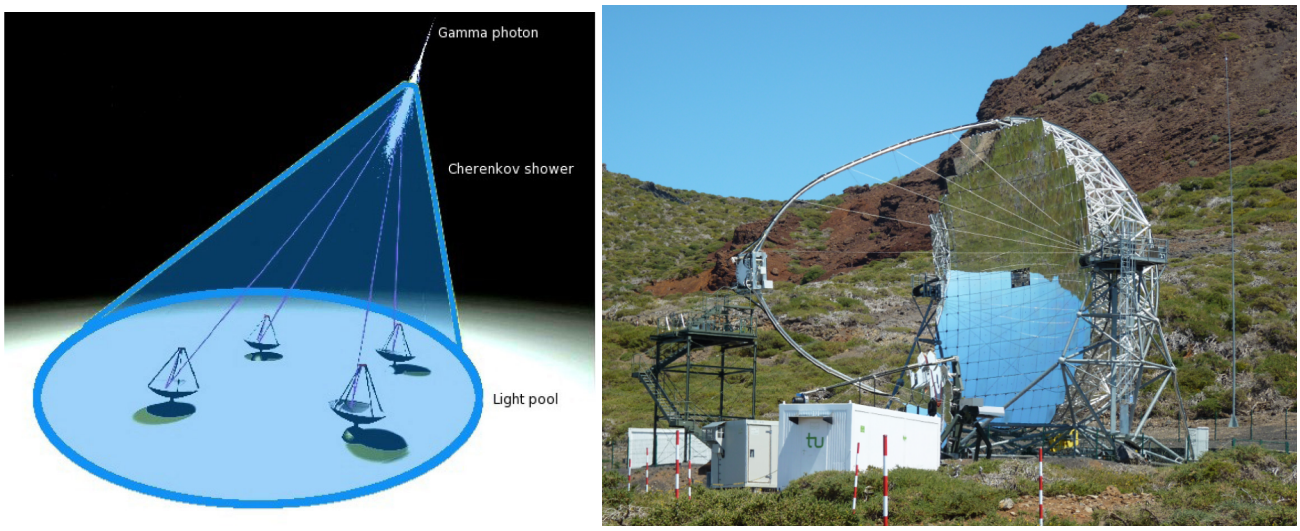

Figure 1.7: Left: the principle of operation of Cherenkov telescopes. RIght: one of the two Cherenkov telescopes of MAGIC stereo pair.

one obtains a conversion between different time-distance units:

$$1 \text{ s} = 3 \times 10^{10} \text{ cm} \tag{1.16}$$

The speed of light serves also for conversion of the units of mass into the units of energy via the relation $E = mc^2$. Thus, any measurement of the mass in grams could be converted into ergs or electronvolts.

The Planck constant relates the energy and frequency of the photon: $E = \hbar\omega$. Setting

$$\hbar = 6.6 \times 10^{-16} \text{ eV s} = 1 \tag{1.17}$$

one obtains a way of measurement of energy in the units of frequency (or inverse time) and vice versa:

$$1 \text{ eV} = 1.5 \times 10^{15} \text{ s}^{-1} \tag{1.18}$$

(notice that the frequency of photons given in the astronomical measurements is usually $\nu = \omega/(2\pi)$, so that the conversion between Hz (frequency of radiation) and eV (energy of photons) differs from the above relation by a 2π factor.

Combining the conversion of centimetres into seconds and seconds into elevtronvolts one finds a relation

$$\hbar c = 2 \times 10^{-5} \text{ eV cm} = 1, \quad \rightarrow \quad 1 \text{ eV} = 5 \times 10^{4} \text{ cm}^{-1} \tag{1.19}$$

In the Natural System of units the electric charge is dimensionless. This is clear from the expression for the fine structure constant:

$$\alpha = \frac{1}{137} = \frac{e^2}{4\pi\epsilon_0\hbar c} = e^2 \tag{1.20}$$

The numerical value of the electron charge is

$$e = \sqrt{\alpha} \simeq 0.085 \tag{1.21}$$

Magnetic field is measured in the units of [energy]^2, as it is clear from the expression for the energy density of magnetic field

$$U = \frac{\mu_0 B^2}{2} = \frac{B^2}{8\pi} \tag{1.22}$$

The energy density is the quantity measured in e.g. [eV/cm^3]. Since cm^{-1} is also an energy unit, the units of U are also [eV^4]. To match the dimensions in the right and left hand side of the above equation, B should be measured in the units of [eV^2]. The conversion between Gauss (the units of magnetic field in the CGS system) and eV^2 could be found from the relation

$$U_B = \frac{[B/1\ \mathrm{G}]^2}{8\pi}\frac{\mathrm{erg}}{\mathrm{cm}^3} \tag{1.23}$$

Taking into account the conversion between the energy units ergs and eV

$$1\ \mathrm{eV} = 1.6 \times 10^{-12}\ \mathrm{erg} \tag{1.24}$$

one finds

$$1\ \mathrm{G} \simeq 0.07\ \mathrm{eV}^2 \tag{1.25}$$

The conversion between Tesla (magnetic field units in the International System) and Gauss is

$$1\ \mathrm{T} = 10^4\ \mathrm{G} \tag{1.26}$$

Combining the last and before-last equations one gets a conversion between Tesla and eV^2.

Other useful conversion coefficients which are needed to bring the astronomical and particle physics data to the common system of units are

- energy/power

$$\begin{aligned} 1\ \mathrm{J} &= 10^7\ \mathrm{erg} = 6.25 \times 10^{18}\ \mathrm{eV} \\ 1\ \mathrm{Jy} &= 10^{-23}\ \mathrm{erg}/(\mathrm{cm}^2\ \mathrm{s\ Hz}) \end{aligned} \tag{1.27}$$

- distance

$$\begin{aligned} 1\ \mathrm{pc} &= 3 \times 10^{18}\ \mathrm{cm} \\ 1\ \mathrm{AU} &= 1.5 \times 10^{13}\ \mathrm{cm} \\ 1\ \text{Å} &= 10^{-8}\ \mathrm{cm} \end{aligned} \tag{1.28}$$

- mass / energy

$$\begin{aligned} 1M_\odot &= 2 \times 10^{33}\ \mathrm{g} \simeq 1.8 \times 10^{54}\ \mathrm{erg} \simeq 10^{66}\ \mathrm{eV} \\ m_e &= 0.9 \times 10^{-27}\ \mathrm{g} = 5 \times 10^5\ \mathrm{eV} \\ m_p &= 1.7 \times 10^{-24}\ \mathrm{g} = 0.94 \times 10^9\ \mathrm{eV} \end{aligned} \tag{1.29}$$

- cross section

$$1\ \mathrm{barn} = 10^{-24}\ \mathrm{cm}^2 \tag{1.30}$$

This set of conversion formulae will be systematically used in numerous numerical estimates encountered in the following chapters.

One important note concerns the gravitational force and Newton constant. From the expression of the Newton's law

$$ma = \frac{G_N M m}{r^2} \tag{1.31}$$

it is clear that the dimensionality of the Newton constant is [mass]$^{-2}$ or, equivalently, [length]^2. This means that it is not possible to set this constant to one in the Natural System of units. Instead, the numerical value of the Newton constant is

$$G_N = 6.7 \times 10^{-8}\frac{\mathrm{cm}^3}{\mathrm{g\ s}^2} = \frac{1}{(10^{19}\ \mathrm{GeV})^2} = \frac{1}{M_{Pl}^2} \tag{1.32}$$

The energy (or mass) scale entering the Newoton's constant is called the Planck scale.

1.5 Excercises

Excercise 1.1. Estimate the temperature of supernova remnant shell assuming that the kinetic energy of explosion (10^{51} erg) is ultimately "thermalized" within the supernova shell of total mass $1M_{\odot}$.

Excercise 1.2. Estimate the temperature of interstellar medium around a star forming region of 100 pc size in which 100 supernovae have exploded on short time scale.

Excercise 1.3. Find the temperature of a black body of mass about $M_{\odot}$ and radius about 10 km (neutron star) and 1000 km (white dwarf) emitting radiation at Eddington limit $L = 10^{38}$ erg/s.

Excercise 1.4. Using the Natural System of Units, find the mass M of a "quantum black hole", a body for which its gravitational radius $R_g = G_N M$ equals its "Compton-like" wavelength, $\lambda = 1/M$.

Excercise 1.5. Using the Natural System of Units, find the strength of "QED-scale" magnetic field B for which motion of mildly relativistic (velocity $v \sim 1$) charged particles of mass m and charge e has to be described in quantum mechanics framework. This happens when the gyroradius $R_L = m/(eB)$ becomes equal to the "Compton-like" wavelength, $\lambda = 1/m$.

Chapter 2

Radiative Processes

2.1 Radiation from a moving charge

Most of the formulae in this chapter for the radiative processes involving electrons (synchrotron and curvature radiation, Compton scattering and Bremmstrahlung emission) are different applications of the basic formulae for the dipole radiation of an accelerated charge. Taking this into account, this section reminds the derivation of the accelerated charge radiation.

Electromagnetic field is a solution of Maxwell equations [7]

$$\frac{\partial F^{\mu\nu}}{\partial x^{\nu}} = -4\pi j^{\mu}. \tag{2.1}$$

where $x^{\mu} = (t, \vec{x})$ are the four-coordinates and j^{μ} is the four-current. Expressing the electromagnetic field tensor through the 4-potential $F_{\mu\nu} = \partial_{\mu}A_{\nu} - \partial_{\nu}A_{\mu}$, we rewrite the Maxwell equations for the potential in the Lorentz gauge $\partial A^{\mu}/\partial x^{\mu} = 0$ in the form of inhomogeneous wave equation

$$\frac{\partial^2 A^{\mu}}{\partial x_{\nu}\partial x^{\nu}} = 4\pi j^{\mu} \tag{2.2}$$

We are interested in the particular case of a point charge e moving along a trajectory $\vec{r} = \vec{r}_0(t)$. Such a charge creates the 4-current $j^{\mu} = e(\delta(\vec{r} - \vec{r}_0(t)), \vec{v}\delta(\vec{r} - \vec{r}_0(t)))$ where $\vec{v} = d\vec{r}_0/dt$ is the velocity. Solution of the wave equation in a point $\vec{r}$ at the moment of time t is determined by the state of motion of the charge at the moment of time t' implicitly found from the relation

$$t' + \left|\vec{r} - \vec{r}_0(t')\right| = t \tag{2.3}$$

The solution of the system of wave equations for the potential is known to be the Lienard-Wichert potential $A_{\mu} = (\phi, \vec{A})$

$$\phi(r,t) = \left.\frac{e}{(R - \vec{v}\cdot\vec{R})}\right|_{t'}, \quad \vec{A}(r,t) = \left.\frac{e\vec{v}}{(R - \vec{v}\cdot\vec{R})}\right|_{t'}, \tag{2.4}$$

where $\vec{R} = \vec{r} - \vec{r}_0$. Electric and magnetic fields corresponding to this potential could be calculated from relations $\vec{E} = \partial\vec{A}/\partial t - \partial\phi/\partial\vec{x}$, $\vec{B} = (\partial/\partial\vec{x}) \times \vec{A}$. This gives an expression

$$\begin{aligned} \vec{E} &= \frac{e(1-v^2)}{(R - \vec{v}\cdot\vec{R})^3}(\vec{R} - R\vec{v}) + \frac{e}{(R - \vec{v}\cdot\vec{R})^3}\left[\vec{R} \times \left[(\vec{R} - R\vec{v}) \times \frac{d\vec{v}}{dt}\right]\right] \\ \vec{B} &= \frac{1}{R}\left[\vec{R} \times \vec{E}\right] \end{aligned} \tag{2.5}$$

If the velocity of the charge does not change in time, $dv/dt = 0$, the second term is absent and the first term just gives the Coulomb field of the charge, falling as R^{-2} at large distances. Using the rules of Lorentz transformation of electromagnetic tensor, one finds that in this case the magnetic field is absent in the reference system comoving with the charge.

Accelerated motion of the charge $dv/dt \neq 0$ leads to the appearance of an additional term which falls as $1/R$ at large distances. Both electric and magnetic field due to this term are orthogonal to the direction toward the charge. This is the field of electromagnetic wave generated by the accelerated motion. A qualitative understanding of the appearance of electromagnetic wave could be obtained via a simple geometrical calculation, see e.g. [2, 1].

At large distances from the source, $r \gg r_0$, and for non-relativistic charge motion, $v \ll 1$, one could approximate $R \simeq r$. In this case the second term in the expression from the electric field of slowly moving charge could be rewritten in the form

$$\vec{E} \simeq \frac{1}{r}\left[\left[\ddot{\vec{d}} \times \vec{n}\right] \times \vec{n}\right] \tag{2.6}$$

where the dipole moment $\vec{d} = e\vec{r}_0$ and the unit vector $\vec{n} = (\vec{r})/r$ are introduced. The magnetic field in these notations is

$$B \simeq \frac{1}{r}\left[\ddot{\vec{d}} \times \vec{n}\right] \tag{2.7}$$

Both electric and magnetic fields are orthogonal to the direction from the charge to the observation point $\vec{n}$ and they are also orthogonal to each other. Such configuration is typical for the electromagnetic wave propagating in the direction $\vec{n}$. The energy flux carried by the wave is given by the Poynting vector

$$\vec{S} = \frac{\left[\vec{E} \times \vec{B}\right]}{4\pi} = \frac{B^2}{4\pi}\vec{n} \tag{2.8}$$

Substituting the expression for B one finds the flux dI in the solid angle $d\Omega$ in the direction n at an angle θ with respect to the direction of $\ddot{\vec{d}}$

$$\frac{dI}{d\Omega} = (\vec{S} \cdot \vec{n}) = \frac{\ddot{d}^2}{4\pi}\sin^2\theta \tag{2.9}$$

One could see that the intensity of emission is directed in a broad angular range preferentially in the direction orthogonal to the acceleration $\ddot{\vec{d}}$.

Integration of the above expression over $0 < \theta < \pi$ gives ($d\Omega = 2\pi \sin\theta d\theta$)

$$I = \frac{2\ddot{d}^2}{3}. \tag{2.10}$$

This is the Larmor formula for the intensity of dipole radiation by an accelerated charge.

This total power is emitted in the form of photons of different energies. To know the energy distribution, or spectrum, of the radiation we decompose the overall power onto power at a given frequency ω by doing the Fouriver transform. For this we use the formula of Fourier analysis stating that $\int_{-\infty}^{\infty} |f(t)|^2 dt = 4\pi \int_{-\infty}^{\infty} |f(\omega)|^2 d\omega$. This means that in the non-relativistic motion case

$$\int_{-\infty}^{\infty} \frac{dI}{d\Omega} dt = \int_{-\infty}^{\infty} \frac{|\ddot{d}|^2}{4\pi}\sin^2\theta dt = \int_{-\infty}^{\infty} \omega^4 |\hat{d}(\omega)|^2 \sin^2\theta d\omega = \int_{-\infty}^{\infty} \frac{d\hat{I}(\omega)}{d\Omega} d\omega \tag{2.11}$$

and the spectral energy density of radiation at the frequency ω is

$$\frac{d\hat{I}(\omega)}{d\Omega} = \omega^4 |\hat{d}(\omega)|^2 \sin^2\theta \tag{2.12}$$

Here the hat denotes the Fourier transform of the function, e.g.

$$d(t) = \int_{-\infty}^{\infty} e^{-i\omega t}\hat{d}(\omega)d\omega \tag{2.13}$$

For a relativistic charge, one introduces the 4-velocity $u^\mu = dx^\mu/d\tau$ where τ is the proper time along the particle trajectory, and the 4-acceleration $a^\mu = du^\mu/d\tau = (d\gamma/d\tau, d(\gamma\vec{v})/d\tau)$, with $\gamma = 1/\sqrt{1-v^2}$ being the particle gamma factor. The Larmor formula rewritten in the 4-vector notations reads

$$I = \frac{2e^2}{3}a_\mu a^\mu = \frac{2}{3}e^2\left(\left(-\frac{d\gamma}{d\tau}\right)^2 + \left(\frac{d(\gamma\vec{v})}{d\tau}\right)^2\right) \tag{2.14}$$

Expressing the derivative of γ through the derivative of v and substituting $dt/d\tau = \gamma$ one could rewrite the last formula in the form

$$I = \frac{2}{3}e^2\gamma^6\left((\vec{v}\cdot\dot{\vec{v}})^2 + \frac{1}{\gamma^2}(\dot{\vec{v}})^2\right) \tag{2.15}$$

where dot denotes the coordinate time derivative d/dt. The quantity $(\vec{v}\cdot\dot{\vec{v}}) = va_{||}$ is the component of particle acceleration parallel to the velocity. One could introduce also the normal component of the acceleration via relation $\dot{\vec{v}}^2 = a_{||}^2 + a_\perp^2$, so that the Larmor formula becomes

$$I = \frac{2}{3}e^2\gamma^6\left(a_{||}^2 + \frac{1}{\gamma^2}a_\perp^2\right) \tag{2.16}$$

2.2 Curvature radiation

Let us consider a relativistic particle with gamma factor γ moving along a circle of the radius R with the speed v. The angular frequency of such motion is $\omega_0 = v/R$. The only component of acceleration different from zero is $a_\perp = \omega_0 v$. The Larmor formula (2.16) gives the total power of emission (which is minus particle energy loss rate)

$$I = \frac{2}{3}e^2\gamma^4\omega_0 v^2 = \frac{2}{3}\frac{e^2\gamma^4 v^4}{R^2} \tag{2.17}$$

The spectrum of emission from a non-relativistic particle in a circular orbit could be found in a straightforward way. The velocity and acceleration are varying periodically with the period $T = 2\pi/\omega_0$, so that the only non-zero component of the Fourier transform of $d(t)$ is $\hat{d}(\omega_0)$. This means that the emission spectrum (for the non-relativistic motion case) is sharply peaked at the frequency ω_0.

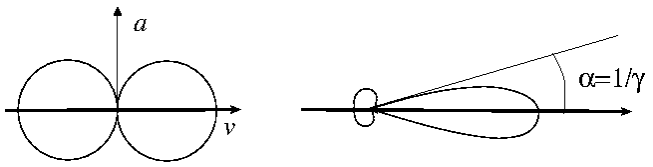

Figure 2.1: Angular pattern of dipole emission from non relativistic (left) and relativistic (right) particles.

The second time derivative of the dipole moment is a vector rotating in the plane of the circular motion of the particle. The angular distribution of the emitted dipole radiation is given by Eq. (2.9) and is shown in the left panel of Fig. 2.1.

In the relativistic case, the angular distribution pattern changes due to the Doppler boosting. To find the characteristic boosting pattern, consider a particle moving along axis x with the speed v close to the speed of light, $v \sim 1$. In the reference system comoving with the particle, particle motion is non-relativistic and emission (e.g. dipole radiation described above) is in a broad range of angles. The transformation to the comoving reference frame has the form

$$x' = \gamma(x - vt); \quad y' = y, \quad z' = z, \quad t' = \gamma(t - vx). \tag{2.18}$$

Transformation of velocities between the laboratory and comoving frame is

$$u_x = \frac{u'_x + v}{1 - vu'_x}, \quad u_y = \frac{u'_y}{\gamma(1 + vu'_x)}, \quad u_z = \frac{u'_z}{\gamma(1 + vu'_x)}. \tag{2.19}$$

Consider a photon which is emitted in the direction normal to the particle motion along y axis in the comoving frame, $u'_x = u'_z = 0$. In the laboratory frame the components of photon velocity are

$$u_x = v, \quad u_y = \frac{u'_y}{\gamma}, \quad u_z = 0 \tag{2.20}$$

The angle between the direction of motion of photon and particle velocity in the laboratory frame is, therefore,

$$\alpha = \frac{u_y}{u_x} = \frac{1}{v\gamma} \simeq \frac{1}{\gamma} \tag{2.21}$$

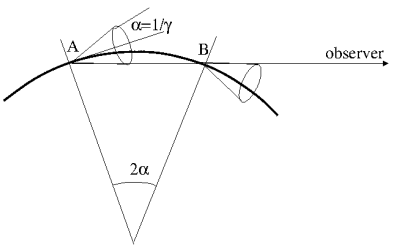

Figure 2.2: Geometry of emission by relativistic particle in circular motion.

A similar estimate, $\alpha \sim \gamma^{-1}$ could be found for the broad range of photon directions in the comoving frame, which are not almost aligned with the direction of particle velocity. Thus, the effect of the Doppler boosting on any broad angle radiation pattern is to compress this pattern into a narrow range of directions $\alpha \lesssim \gamma^{-1}$ around the direction of particle velocity v.

Relativistic beaming also dramatically changes the spectrum of radiation. Consider an observer situated in the plane of circular motion at large distance from the particle. (S)he detects the radiation in the form of short pulses, each time when the beam with an opening angle $\alpha \simeq \gamma^{-1}$ directed along particle velocity passes through the line of sight. The duration of the pulse could be readily calculated from geometry shown in Fig. 2.2. The radiation is visible from a fraction of the circle of particle trajectory spanning an angle 2α. The length of the arc of the angular size 2α is $L = 2\alpha R$ and the time interval during which particle emits in the direction of observer is therefore $\Delta t = 2\alpha R/v$. Suppose that the particle passes the point A at the moment t_0. The photon emitted at this point arrives at the location of observer after a time delay $\delta t_A = d/c$, where d is the distance to the observer. The last photon in the direction of the observer is emitted at the point B, at the moment $t_A = t_0 + \Delta t$. It arrives at the location of the observer at the moment $t_B = t_0 + \Delta t + \delta t_B$, where $\delta t_B = (d - L)/c$. The overall duration of the pulse seen by the observer is

$$\Delta t_{obs} = t_B - t_A = \Delta t + \delta t_B - \delta t_A = \Delta t\,(1 - v) = \frac{2R}{\gamma v}(1 - v) = \frac{2R}{\gamma^3 v(1 + v)} \simeq \frac{R}{\gamma^3} \tag{2.22}$$

where we have substituted $v \simeq 1$ in the last equality. The Fourier transform of the time sequence of pulses detected by the observer has all harmonics up to the frequency

$$\omega_{curv} \sim \frac{1}{\Delta t_{obs}} \sim \frac{\gamma^3}{R} \tag{2.23}$$

It is useful to have a numeric reference value for this frequency for the future estimates:

$$\epsilon_{curv} = \hbar\omega_{curv} = \frac{\hbar c\gamma^3}{R} \simeq 2 \times 10^4 \left[\frac{\gamma}{10^5}\right]^3 \left[\frac{R}{10^6\ \mathrm{cm}}\right]^{-1}\ \mathrm{eV} \tag{2.24}$$

One could understand the above formula in the following way. Relativistic electrons with energies $E_e = \gamma m_e \simeq 100$ GeV confined within a region of the size $R \sim 10$ km, they inevitably emit curvature radiation in the hard X-ray band, at the energies about $\epsilon_{curv} \sim 20$ keV. As an "everyday life" example

of such situation one could mention the past times when the LHC accelerator machine in CERN was still electron-positron collider LEP (Large Electron Positron). It was operating at the energies $E \sim 100$ GeV accelerated in the LHC tunnel of the radius $R \sim 10$ km. From Eq. (2.24) one could find that the electron beam was a source of hard X-rays.

Situation when high-energy particles are confined within an astronomical source of finite size is typical. Thus, generically, all astronomical sources hosting high-energy particle accelerators should be visible in telescopes, because the charged high-energy particles confined within the source emit (at least!) curvature radiation photons.

Particles emitting curvature radiation loose energy at the rate

$$-\frac{dE_e}{dt} = I \simeq \frac{2}{3}\frac{e^2\gamma^4}{R^2} \simeq 4 \times 10^{11} \left[\frac{\gamma}{10^5}\right]^4 \left[\frac{R}{10^6 \text{ cm}}\right]^{-2} \frac{\text{eV}}{\text{s}} \tag{2.25}$$

(see Eq. (2.17)). Once injected in such a compact region of space, TeV electrons loose all their energy within the time interval shorter than one second. Coming back to the LEP example, one could conclude from Eq. (2.25) that supporting the beam of accelerated electrons in the LEP accelerator machine required continuous "re-acceleration" of the beam. All the beam energy was continuously dissipated into the hard X-rays.

2.2.1 Astrophysical example (pulsar magnetosphere)

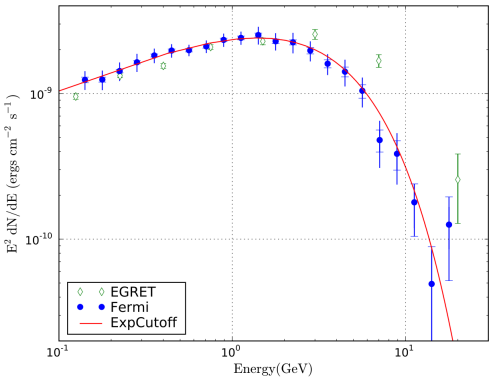

Figure 2.3: Spectrum of pulsed γ-ray emission from Vela pulsar (the brightest GeV γ-ray point source on the sky). From Ref. [8].

The reference example illustrating curvature radiation in astrophysical environments is the currently most often considered model of γ-ray emission from magnetospheres of pulsars.

Pulsars are strongly magnetised and fast spinning neutron stars, i.e. compact stars of the size $R_{NS} \sim 10^6$ cm, rotating at frequencies $1 - 10^3$ Hz and possessing magnetic fields in the range of $B \sim 10^{12}$ G. Most of the isolated point sources of GeV γ-rays in the Galactic Plane are pulsars. Spectrum of emission from the brightest pulsar on the sky, the Vela pulsar, is shown in Fig. 2.3.

The bright GeV γ-ray emission from the pulsars is pulsed at the period of rotation of the neutron stars ($1 - 10^3$ Hz). This implies that the γ-ray photons are produced close to the neutron star, in a region reasonably close to the surface of the neutron star. We adopt a first estimate $R \sim R_{NS} \sim 10^6$ cm and leave further details for the dedicated section on pulsars. This emission is detected at the energies exceeding 1 GeV. It is inevitably produced by relativistic particles.

As it is mentioned above, relativistic particles confined to a compact spatial region inevitably loose energy at least onto curvature radiation (there might be competing energy loss channels, we will consider them later on). Using Eq. (2.24) one could estimate the energies of electrons responsible for the observed γ-ray emission, under the assumption that the γ-rays are produced via curvature mechanism

$$E_e \simeq 2 \times 10^{12} \left[\frac{\epsilon_{curv}}{1 \text{ GeV}}\right]^{1/3} \left[\frac{R}{R_{NS}}\right]^{1/3} \text{ eV} \tag{2.26}$$

Assumption that emission observed in pulsars comes from the curvature radiation process provides, in a sense an upper bound on the energies of particles contained in the sources. Indeed, we will see later on in the course that most of the radiation processes encountered in High-Energy Astrophysics

are different variations of one and the same process of dipole radiation. Each time when trajectories of relativistic particles are deflected by some force, they start to radiate. The slowest possible deflection rate and, respectively, the largest possible extent of particle trajectory is when particle is deviated only when it crosses the entire astronomical source where it is confined. The slowest possible deflection rate leads to the "minimal" energy loss rate and to the emission of lowest energy photons. This is the case of curvature radiation with $R \; R_{NS}$ in pulsars. From these arguments one could conclude that typical energies of electrons confined around pulsars are

$$E_{e,\; pulsars} \lesssim 10^{12} \text{ eV} \tag{2.27}$$

This conclusion just stems from an observational fact that most of the pulsars have high-energy cut-offs in the spectra in the GeV energy band. It does not depend on the details of the model of particle acceleration and interactions which lead to the observed γ-ray emission.

2.3 Evolution of particle distribution with account of radiative energy loss

A competition between acceleration, energy loss and escape processes leads to formation of broad energy distribution of high-energy particles inside astronomical sources

$$\frac{dN_e}{dE} = f_e(E). \tag{2.28}$$

The index e is introduced to distinguish the distribution of charged high-energy particles, e.g. electrons, from the distribution of photons emitted by these particles, which we will denote as dN_γ/dE.

The acceleration process injects particles of energy E with a rate $Q_e(E)$. Then particles are cooling due to radiative and non-radiative losses, with a rate $\dot{E}$, which is also a function of energy. As a result, their energy decreases and $f_e(E)$ at the injection energy decreases, while $f_e(E - \int \dot{E} dt)$ increases. Particles do not disappear once injected, so that the function $f_e(E)$ should satisfy a continuity equation in the energy space

$$\frac{\partial f_e}{\partial t} + \frac{\partial}{\partial E}\left(\dot{E} f_e(E)\right) = Q_e(E,t) \tag{2.29}$$

The sense of this equation is that the increase / decrease of f_e in a unit time in a given energy bin of the width ΔE at reference energy E is given by the rate of injection $Q_e \Delta E$, by the rate influx of particles from the adjacent higher energy bin, $-\dot{E} f(E)\Big|_{E+\Delta E}$ and the rate of outflow into the adjacent lower energy bin $-\dot{E} f(E)\Big|_E$ ($\dot{E} < 0$ is "velocity" along the energy axis, compare with the continuity equation of the fluid dynamics: $\partial f/\partial t + \vec{\nabla}(f\vec{v}) = Q$).

In the above equation, Q is a source of particles, but could also be the "leakage" of particles (then it is negative). The leakage, or escape of particles is often characterised by typical escape time τ_{esc}, which could be a function of energy. Then, the source / leakage term, from dimensional reasons, has the form

$$Q_{e,esc} = \frac{f_e}{\tau_{esc}(E)} \tag{2.30}$$

so that the Eq. (2.29)

$$\frac{\partial f_e}{\partial t} + \frac{\partial}{\partial E}\left(\dot{E} f_e(E)\right) = Q_e(E,t) - \frac{f_e}{\tau_{esc}} \tag{2.31}$$

In the steady state situation, $\partial f/\partial t = 0$, in the absence of escape $\tau_{esc} \to \infty$, the solution of the above equation has the form

$$f_e(E) = \frac{1}{\dot{E}} \int_E^\infty dE' \; Q_e(E') \tag{2.32}$$

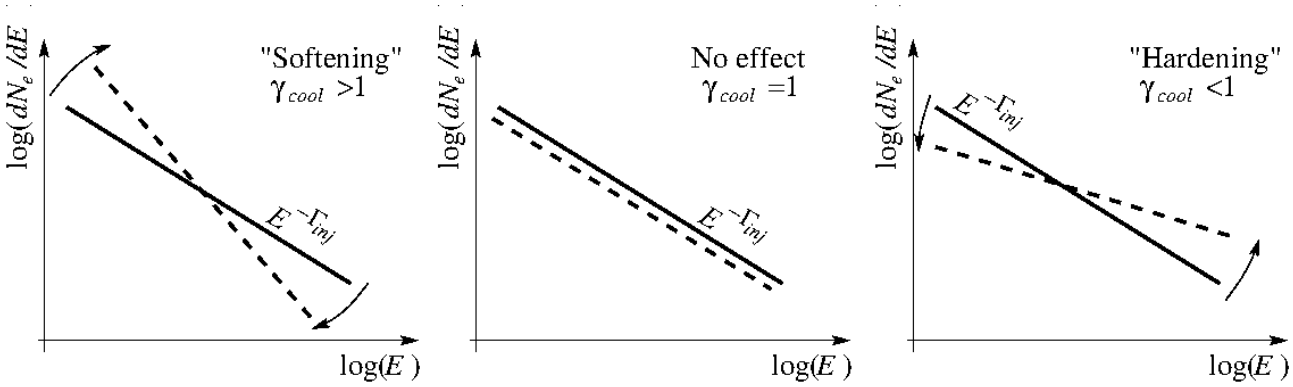

Figure 2.4: The effect of cooling on particle spectrum for different energy dependance of the cooling rate.

As an example, let us calculate the energy distribution of particles reached in the situation where the injection is a delta-function in energy $Q(E) \sim \delta(E - E_0)$. In this case the above solution of the equation takes the form

$$f_e(E) = \begin{cases} 1/\dot{E}, & E < E_0 \\ 0, & E > E_0 \end{cases} \tag{2.33}$$

If the cooling is provided by the curvature radiation, then $\dot{E} \sim E^4$ and

$$f_e(E) = \begin{cases} AE^{-4}, & E < E_0 \\ 0, & E > E_0 \end{cases} \tag{2.34}$$

where A is a normalisation factor. One could see that cooling leads to a "pile up" of particles at lower energies: the number of particles per unit energy interval (or per decade in energy) increases with the decrease of their energy.

In general, if the energy loss rate scales with particle energy as $\dot{E} \propto E^{\gamma_{cool}}$, the effect of cooling on a powerlaw distribution of particles is "softening" or "hardening" of the spectrum, see Fig. 2.4.

2.4 Spectrum of emission from a broad-band distribution of particles

One could see from the previous subsection that typically high-energy particles are distributed over a wide energy range (e.g. form a powerlaw type spectra), rather than concentrate around a particular energy. Broad distribution of energies of emitting particles leads to a broad distribution of energies of emitted photons.

In general, the spectrum of emission from a distribution of electrons (protons) $dN_e/dE = f_e(E_e) \sim E_e^{-\Gamma_e}$ could be calculated once the spectrum of emission from mono energetic electrons $\Phi(E_e, E_\gamma)$ is known. The intensity Φ of emission at the energy E_γ depends on the electron energy E_e. The emission from the distribution of electrons is given by the integral

$$\phi(E_\gamma) = \int \frac{dN_e}{dE_e} \Phi(E_e, E_\gamma) dE_e \tag{2.35}$$

Let us calculate the spectrum of curvature emission from a powerlaw distribution of electrons $dN_e/dE = f_e(E_e) \sim E_e^{-\Gamma_e}$ in the particular case of curvature radiation. Electrons of the energy E_e emit curvature photons of the energy given by Eq. (2.24), $E_{\gamma,*} \sim E_e^3$. In the first approximation one could adopt a "delta-function approximation" for the spectrum of emitted photons, $\Phi(E_e, E_\gamma) \sim$

$\delta(E_\gamma - E_{\gamma,*})$. The normalisation of the emission spectrum is proportional to the rate of emission of photons , given by Eq. (2.25), the emission power, divided by the photon energy $E_\gamma = E_e^3/(m_e^3 R)$.

$$\Phi(E_e, E_\gamma) = \frac{E_e}{m_e R}\delta\left(E_\gamma - \frac{E_e^3}{m_e^3 R}\right) \tag{2.36}$$

Substituting this expression into (2.35) and taking the integral, we find

$$\begin{aligned}
\phi(E_\gamma) &\sim \int E_e^{-\Gamma_e}\frac{E_e}{m_e R}\delta\left(E_\gamma - \frac{E_e^3}{m_e^3 R}\right) dE_e \\
&\sim \int \frac{E_e^{1-\Gamma_e}}{m_e R}\frac{m_e^3 R}{3E_e^2}\delta\left(E_\gamma - \frac{E_e^3}{m_e^3 R}\right) d\left(\frac{E_e^3}{m_e^3 R}\right) \\
&\sim E_e^{-\Gamma_e - 1} \sim E_\gamma^{\frac{-\Gamma_e - 1}{3}}
\end{aligned} \tag{2.37}$$

Thus, the spectrum of emission from a power law distribution of emitting particles is also a power law.

We can generalise the above formula for an arbitrary dependence of the power of emission on the electron energy, $P(E_e) \sim E_e^{\gamma_{cool}}$ ($\gamma_{cool} = 4$ in the case of curvature radiation) and an arbitrary relation between photon and electron energy, $E_{\gamma,*} \sim E_e^\sigma$, ($\sigma = 3$ in the case of curvature emission). This gives

$$\phi(E_\gamma) \sim E_\gamma^{\frac{\gamma_{cool}+1-\Gamma_e-2\sigma}{\sigma}} \tag{2.38}$$

We will reuse this formula to calculate the spectra of synchrotron, Compton and Bremsstrahlung emission in the following sections.

In a particular case when the shape of the particle spectrum is affected by the effects of cooling (see Eq. **??**),

$$\Gamma_e = \Gamma_{inj} + \gamma_{cool} - 1 \tag{2.39}$$

the emission spectrum is independent on the energy scaling of the cooling rate γ_{cool}:

$$\phi(E_\gamma) \sim E_\gamma^{\frac{2-2\sigma-\Gamma_{inj}}{\sigma}} \tag{2.40}$$

Examples of powerlaw (or cut-off powerlaw) spectra of emission from a distribution of high-energy particles could be found in Figs. 2.3, 2.5. Publicaitons in X-ray and γ-ray astronomy often give representation of the spectrum in the form

$$\begin{aligned}
&\frac{dN_\gamma}{dE}(E_\gamma) \sim \phi(E_\gamma), \text{ "differential spectrum" or} \\
&E_\gamma\frac{dN_\gamma}{dE}(E_\gamma) \sim E_\gamma\phi(E_\gamma), \text{ "photon spectrum" or} \\
&E_\gamma^2\frac{dN_\gamma}{dE}(E_\gamma) \sim E_\gamma^2\phi(E_\gamma), \text{ "spectral energy distribution"}
\end{aligned} \tag{2.41}$$

The first representation for the photon flux, in units of "photons/(cm^{2}s eV)" is called the "differential spectrum", i.e. it is the photon count rate per unit detector area per unit time and *per unit energy interval*. The second representation provides a fair judgement of the signal statistics in different energy bands, because it gives the count rate of photons per unit detector area *per decade of energy*. Finally, the third representation, often called "Spectral Energy Distribution" or SED of the source, provides an estimate of the " emitted power per energy decade". This representation is useful for building physical models of the sources. It allows to judge in which energy band most of the source power is emitted.

Cooling law:		$\dot{E} \propto E_e^{\gamma_{cool}}$
Relation between photon and electron energies:		$E_\gamma \propto E_e^{\sigma}$
Electron spectrum:		$dN_e/dE_e \propto E_e^{-\Gamma}$
Emission spectrum:		$dN_\gamma/dE_\gamma \propto E_\gamma^{\frac{\gamma_{cool}+1-\Gamma_e-2\sigma}{\sigma}}$
Evolution of electron spectrum:		$\Gamma_{inj} \to \Gamma_{inj} + \gamma_{cool} - 1$
	γ_{cool}	σ
curvature radiation	4	3
synchrotron radiation	2	2
inverse Compton (T)	2	2
inverse Compton (KN)	0	1
Bremsstrahlung	1	1

2.5 Excercises

Excercise 2.1. Use the expression for the intensity of radiation from a relativistically moving charge (2.16) for an order-of-magnitude comparison of contributions due to the first and second term for an ultra-relativistic particle moving with veolcity $v = 1 - \epsilon$, $\epsilon \ll 1$, experiencing acceleration on a time scale $t = 1/\omega_0$. Which term dominates: the one proportional to $a_{||}$, or the one proportional to $a_\perp$?

Excercise 2.2. By analogy with the astrophysical example of curvature radiation from pulsar magnetosphere, consider the possibility of curvature radiation from a magnetosphere of a black hole in an Active Galactic Nucleus (AGN) of M87 galaxy. The black hole mass is $M \sim 4 \times 10^9 M_\odot$ and the characteristic distance scale in the source is the gravitational radius R_g (see. Excercise 1.4). γ-rays with energies up to 10 TeV are detected from M87 (see Fig. 2.5). Using this information find an upper bound on energies of electrons and protons present in the source. Find a characteristic curvature radiation energy loss time scale $t_{curv} = E/I_{curv}$ for electrons and protons of energy E. Is it shorter or longer than the "light-crossing" time scale $t_{lc} = R_g/c$?

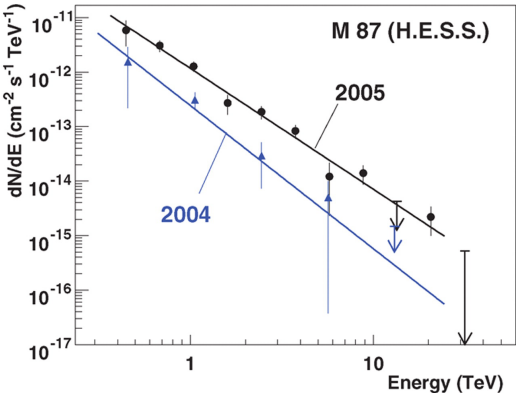

Figure 2.5: Spectrum of γ-ray emission from vicinity of supermassive black hole in M87 galaxy, from Ref. [9].

Excercise 2.3. Find steady-state spectrum of high-energy particles injected at a constant rate with a powerlaw spectrum $Q_e(E) \sim E^{-\Gamma_{inj}}$ and cooling due to a radiative energy loss with the energy loss rate which scales as powerlaw of particle energy: $\dot{E} \sim E^{\gamma_{cool}}$.

Abbreviations

AGN	Active Galactic Nucleus
FR I, FR II	Fanaroff-Riley radio galaxy, type I or type II
GRB	Gamma-Ray Burst
HMXRB	High-Mass X-ray Binary
LMXRB	Low-Mass X-ray Binary
PSR	Pulsar (name in astronomical catalogues)
PWN	Pulsar Wind Nebula
QSO	Quasi-Stellar Object (name in astronomical catalogues)
SNR	Supernova Remnant
Sy I, Sy II	Seyfert galaxy, type I or II
XRB	X-Ray Binary

Bibliography

[1] T.Courvoisier, *High-Energy Astrophysics*, Springer 2013.

[2] M.Longair, *High-Energy Astrophysics*, Third Edition, Cambridge Univ. Press, 2011.

[3] F.Aharonian, *Very High Energy Cosmic Gamma Radiation*, World Scientific, 2004.

[4] J. Beringer et al. (Particle Data Group), Phys. Rev. D86, 010001 (2012).

[5] T.Courvoisier, A&AR, 9, 1 (1998).

[6] J.Jackson, *Classical Electrondynamics*, Wiley & Sons, 1962.

[7] L.D.Landau, E.M.Lifshitz, *The Classical Theory of Fields*, Pergamon Press, 1971.

[8] Abdo A.A. et al., Ap.J., 696, 1084, 2009.

[9] Aharonian F. et al., Science, 314, 1424, 2006.

[10] Kreykenbohm I., et al., A&A, 433, L45, 2005.

[11] Hester J.J. ARA&A, 46, 127, 2008.

[12] Tavani M. et al., Science, 331, 736, 2011.

[13] Berezinsky V., Nucl.Phys.Proc.Suppl.188, 227 (2009) [arXiv:0901.0254]

[14] Ackermann M., et al., Ap.J., 750, 3 (2012).

[15] Ackermann M., et al., Science, 334, 1103 (2011).

[16] Berger E., ARA&A, 51, 43 (2014).

[17] S.Lee, Phys.Rev. D58, 043004 (1998).

[18] K.A. Olive et al. (Particle Data Group), Chin. Phys. C, 38, 090001 (2014)

[19] Yakovelv & Petchik, ARA&A, 42, 169 (2004)